Spectral dynamics of a free-electron maser with a step-tapered undulator

P. J. Eecen, T. J. Schep, and A. V. Tulupov*
FOM–Instituut voor Plasmafysica "Rijnhuizen," Associatie EURATOM-FOM
Postbus 1207, 3430 BE Nieuwegein, The Netherlands
(Received 17 March 1995)

The spectral behavior of a high-power, high-gain free-electron maser (FEM) is investigated. The maser has a step-tapered undulator consisting of two sections with different strengths and lengths and equal periodicities. The sections are separated by a field-free gap. The configuration is enclosed within a low quality cavity. The millimeter wave beam is guided within a rectangular corrugated waveguide. The purpose of this undulator setup is to enhance the efficiency at high output power. The associated high gain in the linear as well as in the nonlinear regime provides a unique oscillator. The spectral dynamics of this device is analyzed with a multipass, multifrequency code. The radiation field of the code is described as a sum over discrete frequency components. The linear gain curve of the step-tapered undulator is not the sum of the curves of two single undulators and has a completely different spectrum. The gain of the FEM is so high that nonlinear interaction occurs within a few passes. In the fully nonlinear regime the gain is still relatively high. The power spectrum evolves towards a state in which the power at the resonance of the second undulator section is suppressed. In the final state, where the frequency spectrum hardly changes from pass to pass, the power spectrum exhibits two peaks at frequencies that are determined by the first section of the undulator. The main peak is related to its resonance frequency, while the second peak is a lower sideband. The dependence of the sideband on the gap length, the relative polarization of both sections, and the reflection coefficient is investigated.

PACS number(s): 41.60.Cr, 41.85.Lc, 52.35.Mw, 52.75.Ms

I. INTRODUCTION

The free-electron maser (FEM) is a free-electron laser (FEL) with wavelengths in the millimeter range. A high-power source in this range is of interest for application in next-generation magnetic confinement reactors for thermonuclear fusion, for example, in the International Thermonuclear Experiment Reactor (ITER). In these reactors the microwave beam is injected for heating and current drive and to assist plasma start-up. For this purpose the microwave source should fulfill the following requirements: a fast tunable frequency between 200 and 250 GHz, a narrow frequency spectrum, a high cw output power of 1 MW, and an overall efficiency exceeding 35%. The start-up of ITER plasmas in the low-field regions by electron cyclotron resonance heating requires 130 GHz. Ignition is reached by heating the core of the plasma at 170 to 230 GHz. Therefore it is essential that the frequency can be tuned from 130 to 230 GHz in a few minutes and over several percent on millisecond scale. Such a source [1] is under construction at the FOM–Institute for Plasma Physics "Rijnhuizen" and will be used for heating and current drive on the Rijnhuizen tokamak RTP and the TEXTOR experiment at Jülich, Germany. In order to meet the frequency requirements, the energy of the electrons is around 1.75 MeV. The high rf power output can be reached with an electron current of 12 A. The FEM is equipped with a decelerator and a depressed collector for recovering the charge and unspent energy of the electron beam. This yields a high overall efficiency.

A key element of the present design is a step-tapered undulator, which is essential in order to provide simultaneously a high linear gain and a high efficiency. The first section provides a large linear gain and the second section of the undulator serves as an amplifier. The step-tapered undulator consists of two planar wigglers with different strengths and lengths. The two sections have the same constant undulator period and polarization. The first section consists of 20 periods of 4 cm and a peak magnetic field of 2.0 kG and the second section consists of 14 periods and a peak magnetic field of 1.6 kG. In order to reduce current losses, each undulator has matching cells at both ends. These cells cause the wiggle motion to be symmetrical with respect to the undulator axis. They have lengths of half an undulator period and strengths of $\frac{1}{4}$ and $\frac{3}{4}$ of the nominal undulator strength. Arrays of correction magnets provide adjustable focusing forces on the electron beam in both transverse directions. The undulator sections are separated by a variable field-free gap.

The low quality cavity consists of a waveguide with mirrors formed by partially reflecting structures. The oversized, rectangular waveguide with internal dimensions of $15 \times 20\,\mathrm{mm}^2$ has corrugated vertical sides. The corresponding millimeter wave field in this waveguide is represented by plane polarized HE_{mn} modes. These modes are peaked at the center resulting in a strong coupling between the electron beam and the microwave

*Present address: Russian Research Centre "Kurchatov Institute," Moscow 123182, Russia.

beam. This waveguide has low losses, as required for the high average power of the FEM. The reflection coefficient of the mirrors is about 0.3 and has a profile with a half-width of about 7 GHz. This coefficient is sufficiently low to keep the intracavity power within reasonable limits, in order to avoid gas breakdown and high Ohmic losses. The peak value of the reflection coefficient can be changed during operation. Even in the stationary regime the gain is high because of the large outcoupled fraction per pass. As a consequence, the microwave field varies considerably over the undulator.

In order to analyze the spectral behavior of the nonlinear interaction between the electron and microwave beam a multifrequency FEL code (MFF) [2] is developed. This is a particle pushing code and is described in the Appendix. The different feature of this code is that the microwave field is described as a sum over discrete modes. These modes are equally spaced in wavelength and all have the same phase velocity. Each mode gives a resonant contribution to the current and charge distribution in the Maxwell equations. The gain mechanism in the FEM can be described by the motion of the electrons in a single ponderomotive potential defined by the undulator field and the total high frequency field. In the MFF code all frequency components contribute to this well (bucket). This is in contrast to single-frequency codes, where the interaction region is divided in several buckets [3].

An important question is the evolution of the spectrum of the FEM with a step-tapered undulator. With the MFF code the dynamics of the frequency spectrum, starting from noise, is analyzed into the nonlinear regime. The linear gain of the total system is appreciably larger than the cumulative gain of the separate sections. Although the main peak is still related to the fundamental resonance of the first undulator, it is strongly modified by the presence of the second one. This linear gain regime exists only during a few passes because of the high gain of the device.

In the nonlinear regime the peak of the fundamental resonance in the first undulator grows strongly, while the peaks at higher frequencies are suppressed. Hence the second section of the undulator starts operating as a pure amplifier of the field generated in the first section. When the power grows beyond a certain value a sideband is generated at the lower frequency side of the surviving peak. No sideband is generated at higher frequencies. It can be concluded that the gain distribution of the first section determines the power spectrum of the step-tapered undulator, while the second section operates as a pure amplifier.

This paper is organized as follows. In Sec. II the model used in the calculations is discussed. The multifrequency description of the microwave field is treated in some detail.

In Sec. III the numerical results are presented and the dynamics of the spectrum is analyzed. Here the profile for the reflection coefficient is taken to be wavelength independent. The evolution of the main peak and the sideband in the spectrum is discussed and a comparison is made with spectra generated with a single undulator.

In Sec. IV the influence of several parameters on the spectrum is investigated. The influence of a wavelength-dependent reflection coefficient is investigated. When the profile is narrow enough the sidebands at both sides of the main peak are suppressed. The important impact of the suppression of the sidebands is the drop of power of the main peak in the frequency spectrum. Furthermore, the gap length is varied and the relative polarization of both sections is changed. It is shown that for different gap lengths the spectra can go from stable to chaotic. Even in the chaotic case, the sidebands at higher frequencies are suppressed. Finally, in the Appendix the MFF code is described.

II. DESCRIPTION OF THE MULTIFREQUENCY FIELD

In this section we will discuss the basic equations that govern the FEM dynamics. The FEM generates microwave pulses longer than 1 ms. Hence the electron beam, as well as the radiation field, may be treated in the continuous beam limit.

The electromagnetic field in the device is given by the sum of an undulator field and a high frequency field. The field of the planar undulator is described by

$$\boldsymbol{a}_u(x,y,z) = -\hat{\mathbf{e}}_x a_{ux}(x,y,z)\cos k_u z, \tag{1}$$

where $k_u = 2\pi/\lambda_u$ is the wave number and λ_u is the period of the undulator. The electron beam propagates in the positive z direction and executes small transverse excursions due to the undulator field. Arrays of correction magnets, placed at the sides of the main wigglers, focus the electrons toward the axis. Close to the axis the forces are approximately linear and the transverse dependence of the undulator field is

$$a_{ux}(x,y,z) = \frac{eB_u(z)}{m_e c k_u}\left(1 + \frac{k_x^2 x^2}{2} + \frac{k_y^2 y^2}{2}\right), \tag{2}$$

where m_e is the electron mass, $e = |e|$ the electron charge, and c the speed of light in vacuum. The transverse undulator wave numbers satisfy the relation $k_x^2 + k_y^2 = k_u^2$. The on-axis field strengths of the two sections and their matching cells are given by

$$B_u(z) = B_{u1}\sum_{i=1}^{5} f_i(h(z - z_{i-1}) - h(z - z_i)) - B_{u2}\sum_{i=1}^{5} f_i(h(z - z_{i+5}) - h(z - z_{i+6})), \tag{3}$$

where B_{u1} and B_{u2} are the maximum wiggler fields of the separate sections, $h(z)$ is the Heaviside function, and $f_1 = f_5 = \frac{1}{4}$, $f_2 = f_4 = \frac{3}{4}$, and $f_3 = 1$. The positions z_i along the z axis are indicated in Fig. 1. Note that the polarization of the wiggler field of the second section is opposite that of the first section. The different field strengths of the two sections lead to different resonance

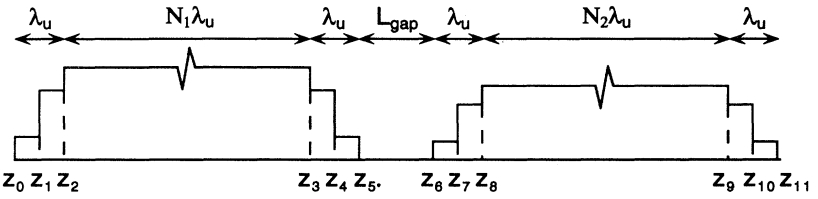

FIG. 1. Sketch of the step-tapered undulator with matching cells.

conditions. For the smaller field strength of the second section, the longitudinal beam velocity v_z is larger and, as a consequence, the beam line $\omega = (k_z + k_u)v_z$ in the dispersion diagram has a steeper slope, leading to a larger resonant frequency (see Fig. 2).

The high frequency field of the maser is denoted by a_L. The polarization of this field is the same as that of the undulator field, i.e., in the x direction. The transverse structure of the field is given by the HE_{mn} eigenmodes of the corrugated waveguide,

$$\boldsymbol{a}_L(x,y,z,t) = \hat{\mathbf{e}}_x \sum_{m,n} a^{mn}(z,t) a_{mn}(x,y), \tag{4}$$

where $a_{mn}(x,y) = \cos(m\pi x/b)\cos(n\pi y/a)$, a and b are the dimensions of the rectangular waveguide, and n and m are odd integers.

The field $a^{mn}(z,t)$ is expressed as a discrete sum over longitudinal cavity modes with frequencies $\omega_l = (1 + l/N)\omega_0$, where l labels the mode. All frequencies are assumed to be close to the reference mode ($l \ll N$). The corresponding wavelengths fit $N+l$ times in the cavity. The reference frequency is $\omega_0 = 2\pi v_{\mathrm{ph}}/\lambda_{z0}$, where $N\lambda_{z0} = L_{\mathrm{cav}}$ with $N \gg 1$, L_{cav} is the cavity length, and $v_{\mathrm{ph}} = \omega_0/k_{z0}$ is the phase velocity. The reference frequency ω_0 satisfies the dispersion relation of the aforementioned waveguide

$$\frac{\omega_0^2}{c^2} = k_{z0}^2 + \left(\frac{m\pi}{b}\right)^2 + \left(\frac{n\pi}{a}\right)^2. \tag{5}$$

The waveguide dispersion curve (5) is plotted in Fig. 2. For all longitudinal modes the phase velocity $v_{\mathrm{ph}} = \omega_l/k_{zl}$ is taken to be equal. This means that each set (ω_l, k_{zl}) satisfies the dispersion relation (5) up to order $O(l[(m\pi/b)^2+(n\pi/a)^2]/(k_{z0}^2N))$. The factor $((m\pi/b)^2+(n\pi/a)^2)/k_{z0}$ is of order 4×10^{-3} and l/N is smaller than 10^{-1}. As can been seen from Fig. 2, the waveguide and the beam line dispersion curves have two intersections. However, it is valid to consider only the phase velocity corresponding to the star in the figure, since the other intersection is far from resonance and will not affect the interaction. In addition, the cross sections of the various frequencies are all on a line, with only small deviations from $v_{\mathrm{ph}} = \omega_0/k_{z0}$.

The cavity modes are described as a product of rapid phase factors and slowly varying amplitudes $a_l^{mn}(z)$

$$a^{mn}(z,\bar{z}) = \sum_{l \ll N} a_l^{mn}(z) e^{\mathrm{i}(1+l/N)k_{z0}\bar{z}}, \tag{6}$$

where $\bar{z} = z - v_{\mathrm{ph}}t$. In the following we will use $(z,\bar{z})$ as coordinates instead of (z,t). The field $a^{mn}(z,\bar{z})$ is $N\lambda_{z0}$ periodic in the $\bar{z}$ coordinate and assumed to be slowly varying in z, i.e., $|\partial_z a_l^{mn}(z)| \ll |k_{zl} a_l^{mn}(z)|$, where ∂_z denotes the partial derivative with respect to z.

The current distribution, which is the source term in Maxwell's equations, is given by adding the contributions of all electrons. With the approximation that the generalized momentum p_x and laser field a_L are small with respect to the undulator field $p_x, a_L \ll a_u$, so that $v_x \simeq a_u/\gamma$, the current distribution can be written as $\boldsymbol{J} = -e\sum_j \delta(\boldsymbol{x} - \boldsymbol{x}_j)\boldsymbol{a}_u/\gamma$, or in the $(z,\bar{z})$ coordinates as

$$J_x = ev_{\mathrm{ph}} \sum_j \frac{1}{\gamma_j \beta_{zj}} \delta(\bar{z} - \bar{z_j}) \times \delta(\boldsymbol{x}_\perp - \boldsymbol{x}_{\perp j})\, a_{ux}(x_j, y_j, z)\cos k_u z, \tag{7}$$

where ϵ_0 is the electric constant, γ the Lorentz factor for the electrons, and β_z the normalized longitudinal velocity of the electrons. We recall that the z dependence of a_{ux} is given in Fig. 1.

Although space charge effects play an important role in the physics of the FEM, it is clarifying first to analyze the nonlinear evolution of the spectrum of a step-tapered undulator in the Compton limit. The Raman FEM will be dealt with in a future paper.

By substituting the current distribution (7) and the field (4) and (6) into Maxwell's equations and integrating over the transverse coordinates we obtain the wave equation

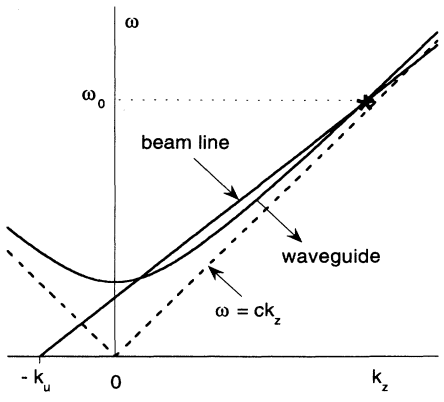

FIG. 2. Waveguide and beam line dispersion curves. The star marks the intersection being investigated.

$$\left[2\left(1+\frac{l}{N}\right)k_{z0}\partial_z + 2i\left(1-\beta_{\rm ph}^2\right)\frac{l}{N}k_{z0}^2\right]a_l^{mn}(z)$$

$$= \frac{8i}{ab}\frac{e}{m_e\epsilon_0 c^3}\frac{I}{N_p}\sum_{j=1}^{N_p}\frac{e^{-i(1+l/N)k_{z0}\bar{z}_j}}{\gamma_j\beta_{zj}}a_{mn}(x_j,y_j) \times a_{ux}(x_j,y_j,z)\cos k_u z. \quad (8)$$

Terms of order $O((1-\beta_{\rm ph}^2)k_{z0}^2 l^2/N^2)$ and the second-order derivative of the slowly varying amplitude $a_l^{mn}(z)$ are neglected in the wave operator. The normalizing factor is the electron beam current I, defined as $I/N_p = ev_{\rm ph}/N\lambda_{z0}$, where N_p is the total number of electrons in the device. Note that the source term in (8) vanishes in the gap between the two undulator sections.

The electron motion in phase space is given by a Hamiltonian system of equations of motion. Taking the longitudinal position z as the free parameter along the particle trajectory, the variables are $(p_x, p_y, x, y, \gamma, \bar{z})$ and the Hamiltonian is given by $\gamma\beta_z$,

$$\gamma\beta_z = \left\{\gamma^2 - \left[1 + p_x^2 + p_y^2 + 2p_x a_{ux}(x,y,z)\cos k_u z + \frac{1}{2}a_{ux}^2(1+\cos 2k_u z) - 2a_{ux}(x,y,z)\cos k_u z \times {\rm Re}\left(\sum_l\sum_{m,n} a_{mn}(x,y)a_l^{mn}(z)e^{ik_{zl}\bar{z}}\right)\right]\right\}^{\frac{1}{2}}, \quad (9)$$

where $a_{ux}(x,y,z)$ is the undulator field given by Eq. (2) and p_x and p_y are the generalized momenta normalized to $m_e c$. The only approximation that has been applied to the Hamiltonian is $a_L^2 \ll a_u^2$. The corresponding equations of motion for an electron interacting with the microwave beam are

$$\frac{d\boldsymbol{p}_\perp}{dz} = -\frac{1}{4\gamma\beta_z}\frac{\partial a_{ux}^2(x,y,z)}{\partial \boldsymbol{r}_\perp}(1+\cos 2k_u z) + \frac{p_x}{\gamma\beta_z}\frac{\partial a_{ux}(x,y,z)}{\partial \boldsymbol{r}_\perp}\cos k_u z + \frac{1}{\gamma\beta_z}\frac{\partial a_{ux}(x,y,z)}{\partial \boldsymbol{r}_\perp}2\cos k_u z \times {\rm Re}\left(\sum_l\sum_{m,n} a_{mn}(x,y)a_l^{mn}(z)e^{ik_{zl}\bar{z}}\right), \quad (10)$$

$$\frac{dx}{dz} = \frac{p_x - a_{ux}(x,y,z)\cos k_u z}{\gamma\beta_z}, \qquad \frac{dy}{dz} = \frac{p_y}{\gamma\beta_z}, \quad (11)$$

$$\frac{d\gamma}{dz} = -\frac{\beta_{\rm ph}}{\gamma\beta_z}2a_{ux}(x,y,z)\cos k_u z \times {\rm Im}\left(\sum_l\sum_{m,n} k_{zl}a_{mn}(x,y)a_l^{mn}(z)e^{ik_{zl}\bar{z}}\right), \quad (12)$$

$$\frac{d\bar{z}}{dz} = 1 - \frac{\beta_{\rm ph}}{\beta_z}. \quad (13)$$

In order to describe high-gain cases, when the field varies quite strongly over a wiggler period, standard procedures of averaging the equations of motion over a wiggler period are not allowed. We stress that slippage between electrons and microwave field is included in these equations. This slip is approximately one wavelength every undulator period.

III. NUMERICAL RESULTS

The wave equation (8) and the N_p particle equations (10)–(13) of the step-tapered FEM are solved with the MFF code. The longitudinal integration of the equations is done with the so-called "leapfrog" method. A description of the code is given in the Appendix. Typical parameters of the calculations are $N = 200$, which gives a frequency spacing of about 1 GHz, with the central frequency at 200 GHz. The number of modes l is such that the total gain curve is described, which is typically 50. The number of particles is $N_p = 40N$. The number of steps in the longitudinal direction is typically ten identical steps per undulator period.

The parameters of the system are those of the design of the FOM FEM for fusion applications and are given in Table I. In this section the reflection coefficient is wavelength independent. In Sec. IV a wavelength selective reflection profile will be considered. In this paper, only the HE_{11} mode is taken into account for the transverse dependence of the microwave field.

The first pass starts with equal power (1 W) for all frequencies considered. During the first passes, the power in the microwave beam is relatively small and the FEM is in the linear gain regime. The linear gain curves of the two sections separately are shown in Fig. 3. The dashed line shows the linear gain curve of the first section acting as a single undulator and the dotted line shows the linear gain curve of the second section also acting as a single undulator. The well separated peaks in these linear gain curves have frequencies of 203 GHz and 220 GHz, with values 30 and 4.5, respectively. The actual spectrum of the composite undulator, the solid line in Fig. 3, clearly differs from the sum of the spectra of the independent

TABLE I. Design parameters of the FOM FEM for fusion applications [1], as implemented in the MFF code.

Beam voltage	1.75 MV ($\gamma = 4.42$)
Beam current	12 A
Beam emittance	49π mm mrad
Beam radius	0.92 mm
Peak wiggler field in section 1	2.0 kG
Peak wiggler field in section 2	1.6 kG
Number of undulator periods in section 1	20
Number of undulator periods in section 2	14
Wiggler period	4.0 cm
Gap between wigglers	6.0 cm
Waveguide mode	HE_{11}
Waveguide dimensions	20×15 mm^2
Reflection coefficient	0.29

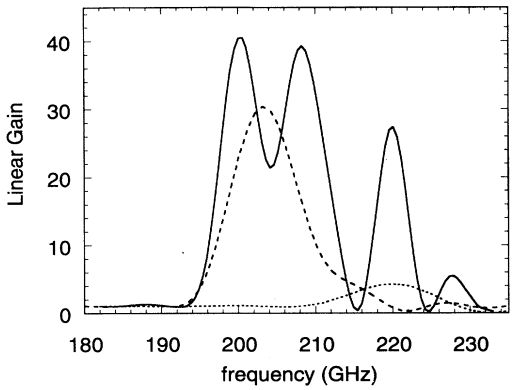

FIG. 3. Linear gain at the end of the first pass as a function of frequency. The solid line is the gain at the end of the first pass through both sections of the undulator with a $1\frac{1}{2}\lambda_u$ gap length. The dashed line is the gain curve of the first section acting as a single undulator and the dotted line is that of the second section acting as a single undulator.

oscillators. This shows that the prebunching of the electrons, as experienced by the second section, is a major effect. The two peaks of the gain curve with the lowest frequencies (200 GHz and 208 GHz) result from the peak of the first undulator, modified by the gap and the second undulator. Clearly, in the composite case the gain is enhanced and the peak of the first section is split. The peak at 220 GHz is generated by the second undulator. Its gain is enhanced due to the prebunching of the electrons in the first section. It can be concluded that the step-tapered undulator is not the sum of two separate systems, but operates as a single system with a significant klystron effect [4].

From the single pass gain curve one might expect that the spectrum evolves into a discrete spectrum with three well distinguished lines with about 10-GHz spacing. However, this is not the case, as will be discussed in the following. The power spectra at the end of the second and third pass, just before the reflection, are plotted in Fig. 4. All results presented in this paper refer to situations just before reflection. The spectra change drastically during these two passes. At the end of the second pass the three peaks in the linear curve of Fig. 3 are evidently still present, but the first peak is already dominant over the other peaks. This peak represents the resonance in the first section. One pass later, the resonance of the second section is suppressed, as can be seen from the dashed line in Fig. 4.

The system has a high linear gain so that already after a few passes the power in the microwave beam becomes large. At this stage the electrons become strongly bunched and the step-tapered undulator begins to operate as a nonlinear system. In this regime the power is reordered over the spectrum and the total power starts to level off. These nonlinear effects are already observed after a few passes, well before the power of the stationary state is reached. In this nonlinear phase the coherent bunching in the first section is strong enough to reduce the second section to an amplifier of the main peak.

The transition from a linear to a nonlinear interaction between the electrons and microwave beam is presented in Fig. 5, where the evolution of the spectrum is shown during the first 60 passes. We recall that with the adopted reflection coefficient, 71% of the power in each frequency component is coupled out per pass. A number of conclusions can be drawn from Fig. 5. After about 10 passes, two peaks in the spectrum survive at the positions of the largest peaks in the linear gain spectrum. The power at the position of the resonant frequency of the second section is orders of magnitude smaller. At a certain power level, one main peak grows from a relatively broad power spectrum. The position of this peak corresponds to the resonant frequency of the first section. The higher frequencies that are generated during the first passes are suppressed during the further evolution of the spectrum. This important effect is observed in all cases. During the first 20 passes, the power is transferred to the

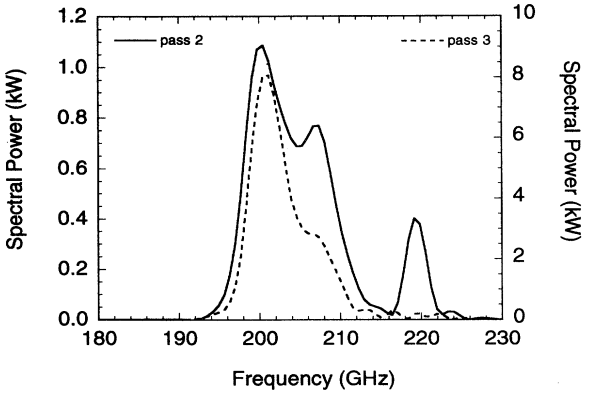

FIG. 4. Power spectrum at the end of the second (solid line) and the third (dashed line) pass.

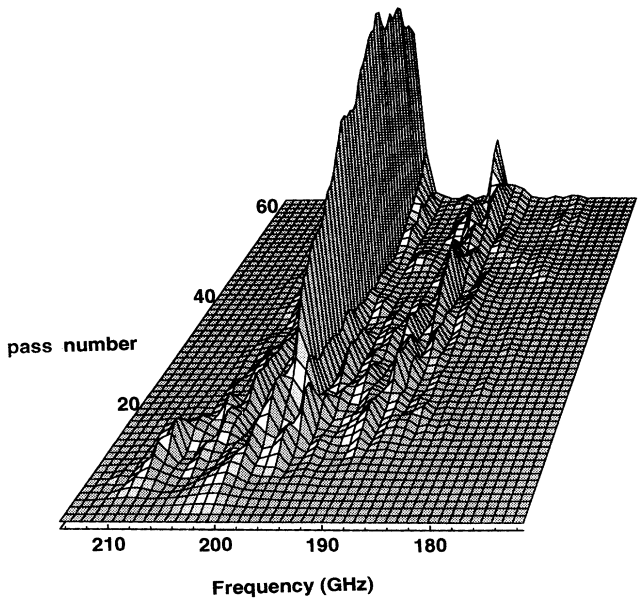

FIG. 5. Evolution of the power spectrum during the first 60 passes for a step-tapered undulator with $1\frac{1}{2}\lambda_u$ gap length.

lower frequencies. This nonlinear process finally results in the generation of a single, lower frequency sideband. Calculations show that during the following passes the sideband exchanges energy with the main signal.

The profile of the power at the end of the 130th pass is plotted in Fig. 6. At that time the system has acquired a double peaked spectrum with the main peak at 199 GHz and a sideband at 188 GHz. The main peak has 1.2 MW of power within a 4-GHz frequency band, while the sideband has 0.4 MW of power within a 5-GHz frequency band. These peaks continue to narrow in frequency.

After 200 passes, the system enters a regime where the spectral structure of the millimeter wave beam stays stable in the sense that the power in the frequency spectrum at the end of each pass does not change during at least the next 200 passes. We will refer to this regime as the stable regime. The spectral power at the end of the 300th pass is plotted in Fig 7. The main peak of the spectrum has a power of 1.3 MW contained within a 1-GHz frequency band. The corresponding sideband is generated at 187 GHz and has a power of 0.5 MW within a 1-GHz band. The total power, i.e., the sum of the power in all frequencies, is 1.92 MW, of which 68% in the main peak and 26% in the sideband. The remaining 6% of the total power is in other frequency components, mainly at the lower frequency side of the main peak.

It is illustrative to compare the previous case with the case where only the first section of the step-tapered undulator is present. The evolution of the spectrum during passes 50 to 150 is plotted in Fig. 8. The figure shows that the system evolves quickly into a stable regime. The main peak is of course determined by the resonance condition and a quite large and well separated sideband is present. Also in this case sideband generation occurs only at the lower frequency side of the main peak. At the end of pass 150, the power of the main peak at 201 GHz is 0.85 MW within a 1-GHz frequency band. The sideband at 190 GHz has a power of 0.3 MW within a 1-GHz frequency band.

It is evident that although their time history is different, the spectrum of the single undulator (Fig. 8) is marginally different from the spectrum of the step-tapered undulator (Fig. 7). However, their power distributions are different. This illustrates again that the second section acts like an amplifier. The spectrum

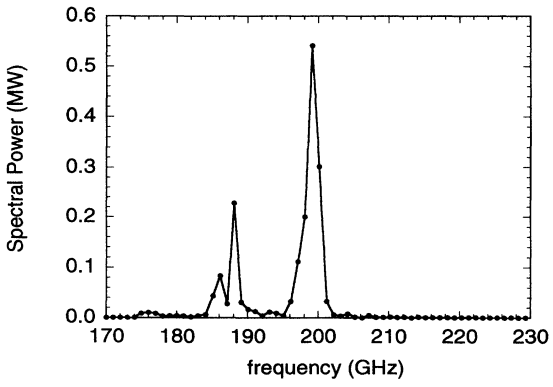

FIG. 6. Power spectrum at the end of the 130th pass.

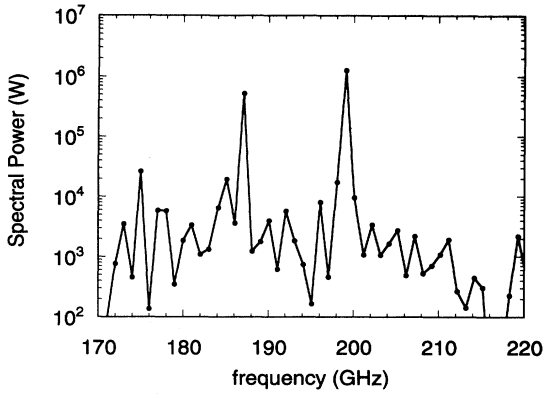

FIG. 7. Power spectrum after 300 passes.

generated by the step-tapered undulator contains more power because amplification of the second section enhances both the power in the main signal and the sideband. The gain in the stable regime of the main signal and the sideband are compared in the first and the second section separately. The gain in the first section is 5–20 times larger, so this section dominates the spectral distribution. In the first section the gain of the main signal is larger than the gain of the sideband, while in the second section the gain of the sideband is larger than the gain of the main signal.

The sideband corresponds to a nonlinear resonance in the system. This resonance is due to the oscillation of the electrons in the potential well generated by the nonlinear interaction between the electrons and the microwave beam. The position of the sideband in the spectrum can

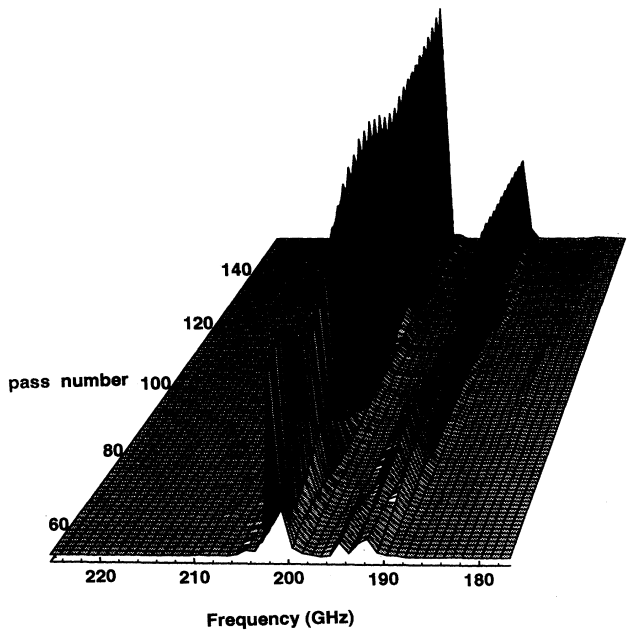

FIG. 8. Evolution of the power spectrum during passes 50–150. The undulator consists of only the first section of the FEM.

be estimated analytically by assuming a monochromatic maser field a_s and a stationary electron distribution. The sideband is then incorporated as a perturbation. When the initial electron distribution is peaked at the bottom of the potential wells, the deeply trapped electrons bounce in the ponderomotive potential with synchrotron frequency $\Omega_{\rm syn}$. This gives rise to sideband growth [5,6]. When applying the resonance condition for a low-energy electron beam, one finds that the position of the sideband is approximately given by

$$\Delta k \simeq \pm \frac{(k_{z0}+k_u)}{k_u}\frac{\Omega_{\rm syn}}{c} \simeq \pm \frac{2(k_{z0}+k_u)}{\beta_z\sqrt{1+a_u^2}}\sqrt{a_u a_s}, \quad (14)$$

where a_u is the normalized undulator field and a_s is the monochromatic maser field of the main peak with wave number k_{z0}.

Multifrequency calculations are performed for a somewhat longer single-section undulator than that used in the calculations in Fig. 8. The undulator has the same parameters as the first section in the FEM, but here 30 undulator periods are taken in order to make overbunching faster and to show the sideband behavior more pronounced. The other parameters are the same and are given in Table I.

The spectral power of the microwave field after the third pass is plotted in Fig. 9. There are clearly two sidebands generated. The estimate for the position of the sideband, given by Eq. (14), is $\Delta\nu \simeq \pm 5$ GHz, which agrees with the positions in the figure. Obviously, the growth rates of the sidebands plotted in Fig. 9 are rather different.

Returning to Fig. 5–8, the most striking result is that the sideband grows only at frequencies lower than the frequency of the main peak. The estimate for the frequency shift of the sideband, given by Eq. (14), is very close to the values observed in these figures.

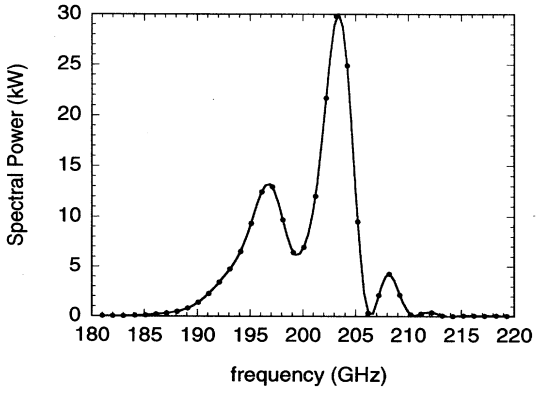

FIG. 9. Power spectrum of an undulator with a single section. The undulator has 30 periods and its parameters are the same as those of the first section of the FEM as given in Table I.

IV. SUPPRESSING THE LOWER SIDEBAND IN A STEP-TAPERED UNDULATOR

An ideal FEM would operate such that all power is confined in a narrow frequency band. Results presented in the previous section have shown that the spectrum involves a sideband, which amplification may lead to an undesired transfer of energy. Therefore, in this section possible means of suppressing this lower sideband will be investigated. The output power and its distribution over the spectrum is scanned as a function of the value of the reflection coefficient, its profile, the gap length and the relative polarization of the undulator sections.

A. Wavelength selective reflection

In the present design of the FEM [1], the reflection coefficient is frequency dependent, with a half-width of approximately 7 GHz. The position of the maximum of the profile is variable. We model this profile by a parabolic shape shown in Fig. 10.

This profile is used to calculate the evolution of the spectrum for a step-tapered undulator with a gap length of $1\frac{1}{2}\lambda_u$. On the basis of previous results (Fig. 7), the maximum value of the reflection coefficient is chosen to be at $\nu_c = 199$ GHz. The power spectrum at the end of the 100th pass is plotted in Fig. 11. At this stage the system is in the stable regime, which is reached much faster than in the case of a constant reflection coefficient. Due to the narrow profile of the reflection coefficient the sideband is suppressed. Compared to the results in Fig. 7, the peak in the power distribution is slightly shifted toward higher frequencies. When the center of the reflection coefficient (Fig. 10) is situated at different positions in the spectrum, the sideband can be more or less suppressed.

An important drawback of the suppression of the sideband by means of a frequency selective reflection coefficient is the drop in power of the main peak. In the case of Fig. 11, the total power is only 0.9 MW, while in the case represented in Fig. 7, the total power is 1.9 MW

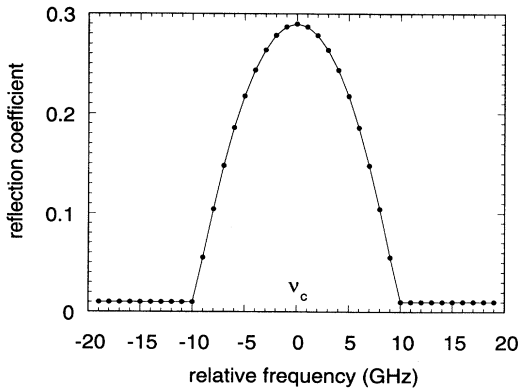

FIG. 10. Model for the profile of the reflection coefficient of the FEM. The center of the curve is at ν_c, which can be chosen freely. The dots represent the $2l$ frequencies of the Fourier modes.

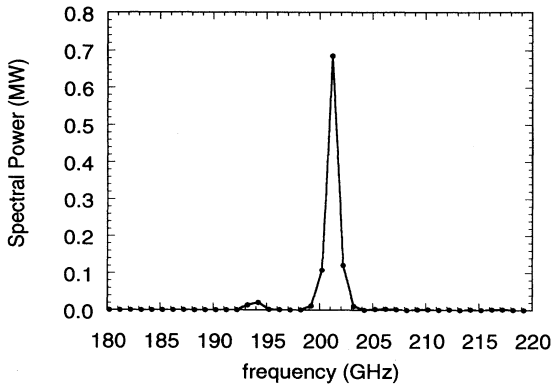

FIG. 11. Power spectrum after the 100th pass for a gap length of $1\frac{1}{2}\lambda_u$ and the profile for the reflection coefficient. The maximum of the reflection coefficient curve is at 199 GHz.

with 1.3 MW in the main peak. Hence, not only does the power in the main peak decrease, but also the efficiency decreases considerably. It can be concluded that the nonlinear interaction is such that the presence of a sideband enhances the power in the fundamental mode. Calculations with other maximum values for the peak value of the reflection coefficient in the range from 0.2 to 0.4 show that the total power in the steady state regime changes by not more than 10%. The history of the stable regime depends strongly on the reflection coefficient, but the final power that is reached is about the same.

A tentative physical model explaining the reduction in power of the main peak is as follows: Analysis shows that in the case of a suppressed sideband, the electrons are overbunched at the end of the first section. Because of this suppression the electrons are not able to cascade into the trapping well at the (lower) resonance energy of the second section. Consequently, at the beginning of the second section the electrons are too far in energy from the trapping well corresponding to the second section and therefore the amplification of the microwave field in the second section is smaller in the steady state, which has been observed in the numerical simulations.

From this perspective, the sideband at the lower frequency side of the main peak can strongly enhance both the total output power as the power of the main peak. This sideband has a lower resonant energy and acts as an intermediary: it serves as a connecting region in phase space between the trapping well of the first section and the lower energy trapping well of the second section, providing a proper electron energy cascade throughout the step-tapered undulator.

B. Variation of the reflection coefficient

We have also investigated cases in which the reflection coefficient is either very large or very small. Flat profiles are considered.

The first section is considered as an independent undulator in two extreme cases. In the case that the reflection coefficient is small, 0.05, the main peak in the spectrum at 203 GHz develops rather slowly. The power saturates at 500 kW at the 300th pass. No sideband is developed. In the second case, the reflection coefficient is large, 0.9. Then the generated spectrum becomes broad. This broadening occurs mainly at lower frequencies than the resonance.

Table II summarizes the results for the step-tapered undulator for a number of reflection coefficients. We find that increasing the reflection coefficient enlarges the power in the stable regime in the main peak as well as in the sideband. The higher frequencies are still suppressed. In all cases of Table II, a large main peak is generated with a sideband at the position given by Eq. (14). For the reflection coefficient of 0.32 the total spectral power is 2.1 MW and the corresponding electron efficiency is 6.9%. At the end of the first section 5.2% of the initial electron energy is transferred into microwave energy.

C. Variation of the gap lengths

In this section the effect of different gap lengths on the spectrum is investigated. For cases with the parameters of Table I and a flat profile for the reflection coefficient, gap lengths of $1\frac{1}{2}\lambda_u$, $1\frac{1}{4}\lambda_u$, and $1\lambda_u$ are considered. It is clear that the linear gain curves depend on the gap length and the corresponding spectra in the nonlinear regime for the various gap lengths are quite diverse.

In all cases the frequencies larger than the main frequency are suppressed. The stable regimes in the cases of $1\frac{1}{4}\lambda_u$ and $1\frac{1}{2}\lambda_u$ gap lengths have the same spectral distributions, which consist of a large main peak and a pronounced sideband. The difference is that the system with a gap length of $1\frac{1}{4}\lambda_u$ reaches the stable regime at higher pass numbers than the system with a gap length of $1\frac{1}{2}\lambda_u$.

In the case of a gap with length $1\lambda_u$, the evolution of the spectrum, however, is much less smooth than in the other cases. There are more peaks in the spectrum and the power in the various peaks can be larger than the power in the main peak. The power distribution can change considerably over a few passes. This chaotic spectral behavior is observed from an early stage and seems

TABLE II. Power of the main peak of the sideband in the steady state regime for different reflection coefficients.

Reflection coefficient R	Main peak power (MW)	Sideband power (MW)
0.23	1.15	0.35
0.26	1.20	0.40
0.29	1.30	0.50
0.32	1.37	0.54

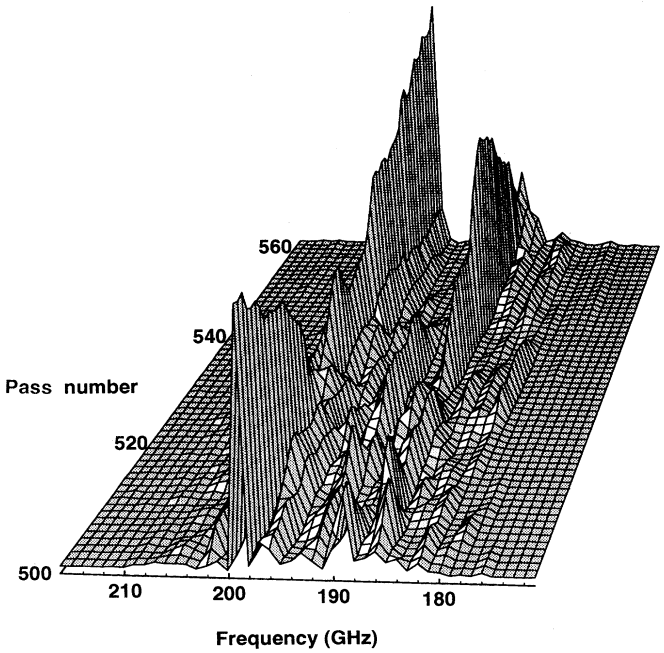

FIG. 12. Evolution of the power spectrum during passes 500–560. The two sections of the undulator are separated by a gap of length $1\lambda_u$.

to remain chaotic at least to the 1000th pass. As an illustration of the chaotic spectral behavior, the evolution of the spectrum between pass 500 and pass 560 is plotted in Fig. 12. Even in this chaotic case the higher frequencies remain efficiently suppressed, but at the lower frequency side of the main peak strong mode competition occurs and even the power in the main peak can occasionally almost vanish.

D. Opposite polarization of the second section

The power spectrum after 150 passes is plotted in Fig. 13 for the case where the two undulator sections

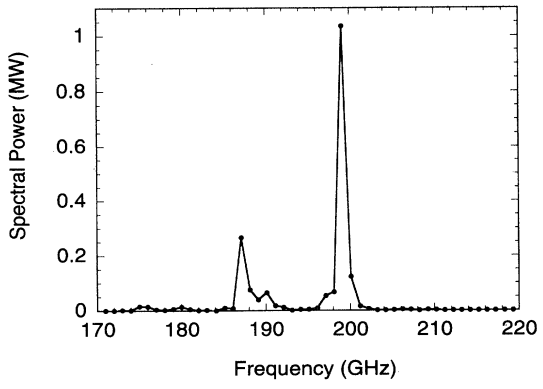

FIG. 13. Power spectrum after the 150th pass with a gap of length $1\frac{1}{2}\lambda_u$ and the same polarization for the second section.

have the same polarization. This means that in Eq. (3) the sign of B_{u2} is changed. The system is in the stable regime and the higher frequencies are again efficiently suppressed. As compared to the case indicated in Fig. 7, the power in the main peak as well as in the sideband is much smaller.

V. CONCLUSIONS

The linear as well as the nonlinear behavior of the step-tapered undulator and the evolution of its spectrum has been studied. The step-tapered undulator operates as a single system with a significant klystron effect. In most cases, the frequency spectrum evolves into a stable regime, in which it hardly changes from pass to pass. In the stable regime a narrow main peak is generated at the resonant frequency of the first section of the undulator. The major part of the total power is confined in this peak. In all cases that are investigated, the spectral power at the resonant frequency of the second section of the undulator is efficiently suppressed. In the nonlinear regime the first section plays a major role in the evolution of the frequency spectrum and the second section acts like an amplifier of the radiation field generated in the first section. When the power in the main frequency is sufficiently high, a strong sideband is generated at the lower frequency side of the main peak. The behavior of the spectrum, in particular the behavior of the sideband, as a function of the value of the reflection coefficient, its profile, the gap length, and the relative polarization of the undulator sections is investigated. Except for the case with a step-tapered undulator with a gap length of $1\lambda_u$, the sideband is quite narrow and contains a substantial part of the total rf power. A reflection coefficient with a sufficiently narrow profile will suppress the sideband, but, as a consequence, the power in the main peak will decrease. In the case of a step-tapered undulator with a $1\lambda_u$ gap length, the stable regime is not reached and the spectrum is quite broad. The power is confined in a 20-GHz interval below the resonant frequency of the first section and behaves chaotically.

ACKNOWLEDGMENTS

This work was performed as a part of the research program of the association agreement of EURATOM and the "Stichting voor Fundamenteel Onderzoek der Materie" with financial support from the "Nederlandse Organisatie voor Wetenschappelijk Onderzoek" and EURATOM.

APPENDIX: THE MULTIFREQUENCY FEL CODE MFF

The multifrequency FEM code MFF calculates the dynamics of the frequency spectrum of the microwave beam interacting with the electron beam, wiggling through the undulator. The system of equations for the individual

electron trajectories and the evolution of the electromagnetic fields in the FEL are self-consistently solved. The code permits the inclusion of many complex physical effects such as nonuniform wigglers and nonideal electron beams. The particle equations of motion are obtained from a Hamiltonian description and the equations for the electromagnetic fields are derived from the Maxwell equations in the slowly varying envelope and phase approximation. The sources in the equations are the current and charge distributions. The paraxial wave approximation has been applied to the electromagnetic fields. The fields are expanded into Fourier harmonics for the cavity modes, therefore the wave equation decomposes into an equation for each mode. The electromagnetic field is described in terms of HE_{mn} waveguide modes. However, the code can treat any waveguide mode. The Maxwell equations solved in the code are ordinary differential equations for each frequency component, given by Eq. (8), that is solved in the longitudinal direction.

The six dimensional phase space for each individual electron is $(\gamma, \bar{z}, p_x, x, p_y, y)$, where γ is the energy, $\bar{z}$ is the position in the pulse, moving with the phase velocity $v_{\rm ph}$, x and y are the radial coordinates, and p_x and p_y are the transverse momenta of the electrons. Therefore, for N_p electrons, $6N_p$ differential equations are solved. The equations of motion (10)–(13) for each individual electron are solved with the Runge-Kutta method. The three-dimensional treatment of the electrons is important for the proper description of the large transverse excursions that the electrons make in the FEM as compared to the standard FEL due to the lower beam energy. This set of equations is supplemented by initial conditions on the phase space variables $(\gamma, \bar{z}, p_x, x, p_y, y)$ at the wiggler entrance and the initial electromagnetic field.

1. Particle loading

The initial conditions at the entrance of the wiggler at $z = 0$ are given in terms of the electron distribution function $\mathcal{F}(\gamma, \bar{z}, p_x, x, p_y, y)$ on the six-dimensional phase space. It is assumed that the distribution $\mathcal{F}$ can be written as $\mathcal{F}_{\bar{z}}(\bar{z})\mathcal{F}_{\gamma}(\gamma)\mathcal{F}_4(p_x, x, p_y, y)$, where $\mathcal{F}_{\bar{z}}(\bar{z})$ is evenly distributed over a fixed number (typically $4N$) of positions in the interval $[0, 2\pi N/k_{z0}]$ in $\bar{z}$ space.

The initial electron energy distribution $\mathcal{F}_{\gamma}(\gamma)$ is Gaussian. The distribution $\mathcal{F}_4(p_x, x, p_y, y)$ is a four-dimensional ellipsoid with minor axes R_x, Δp_x, R_y, and Δp_y, filled with the Hammersley sequence. The initial power and phase of each frequency component and waveguide mode of the microwave field must be defined at the wiggler entrance before the first pass.

2. Integration

The integration of the wave equation is a first-order forward difference scheme that is used to determine the z derivative. The z axis is discretized in intervals with end points at z_{n-1} and $z_n = z_{n-1} + \Delta z$. Furthermore, the center point of each interval is defined as $z_{n-1/2} = (z_n + z_{n-1})/2$. The particle phase space variables are known at positions z_{n-1} and the radiation field at positions $z_{n-1/2}$. Using the solution of the radiation field at $z_{n-1/2}$, the particle equations are advanced from z_{n-1} to z_n, followed by the construction of the Maxwell sources from the new particle variables at z_n. With the new Maxwell sources at z_n, the radiation field at $z_{n-1/2}$ is advanced to $z_{n+1/2}$. In this way the centering at z of the wave equation discretization is ensured.

In the variables $(z, \bar{z})$, where $\bar{z} = z - v_{\rm ph}t$, the radiation field is fixed in $\bar{z}$. The electrons however, have a different velocity v_z. As a result of this difference, the electrons slip approximately one wavelength per undulator period behind the electromagnetic pulse during their transit through the wiggler. The continuous beam limit is considered, which is appropriate for pulses much longer than the slippage length.

[1] W. Urbanus *et al.*, Nucl. Instrum. Methods Phys. Res. Sect. A **318**, 16 (1992); **331**, 235 (1993).
[2] P.J. Eecen, A.V. Tulupov, and T.J. Schep, Nucl. Instrum. Methods Phys. Res. Sect. A **341**, 309 (1994).
[3] W.B. Colson, Nucl. Instrum. Methods Phys. Res. Sect. A **237**, 1 (1985); G.H.C van Werkhoven, B. Faatz, and T.J. Schep, Phys. Rev. E **50**, 4063 (1994).
[4] N.S. Ginzburg and M.I. Petelin, Int. J. Electron. **59**, 291 (1985).
[5] N.M. Kroll, P.L. Morton, and M.N. Rosenbluth, IEEE J. Quantum Electron. **QE-17**, 1436 (1981); M.N. Rosenbluth, H.V. Wong, and B.N. Moore, Phys. Fluids B **2**, 1635 (1990).
[6] R.C. Davidson and J.S. Wurtele, Phys. Fluids **30**, 557 (1987).